AMERICAN JOURNAL of PHYSICS

Onsager symmetry relations and ideal gas effusion: A detailed example

S. N. Patitsas

Citation: American Journal of Physics **82**, 123 (2014); doi: 10.1119/1.4827829
View online: http://dx.doi.org/10.1119/1.4827829
View Table of Contents: http://scitation.aip.org/content/aapt/journal/ajp/82/2?ver=pdfcov
Published by the American Association of Physics Teachers

Onsager symmetry relations and ideal gas effusion: A detailed example

S. N. Patitsas[a)]
Department of Physics & Astronomy, University of Lethbridge, 4401 University Drive, Lethbridge Alberta, Canada T1K3M4

(Received 10 March 2013; accepted 17 October 2013)

Onsager coefficients are calculated for the approach of a gas to equilibrium by effusion between two chambers. Using kinetic gas theory, the Onsager symmetry relation is explicitly verified. The approach to equilibrium is determined by two time scales that are explicitly calculated; this is followed by example calculations for dynamics of the system approaching equilibrium in several ways. Also, calculations for the cross-correlation functions for this system are presented, which are used to calculate various noise spectral functions. This study provides students of statistical mechanics and thermodynamics with a good example to aid in understanding some of the general concepts encountered in studies of non-equilibrium systems.
[http://dx.doi.org/10.1119/1.4827829]

I. INTRODUCTION

In systems containing two or more irreversible transport mechanisms, reciprocal relations among transport coefficients can often be observed. Examples date back to Lord Kelvin's analysis of thermoelectric phenomena and Helmholtz's investigations into the conductivity of electrolytes.[1,2] In 1931, Lars Onsager published his seminal studies concerning the approach to thermodynamic equilibrium.[3,4] This was specifically a linearized theory where it was assumed that the system is not very far from equilibrium and assumptions of local equilibrium apply. Such a linearized approach naturally involves constant coefficients. Onsager showed that there exist general symmetries among such coefficients. This work was further developed theoretically over the next couple of decades,[5–7] while from the experimental side many systems were studied in detail, including systems exhibiting particle diffusion, thermal conduction, electrical conduction, thermoelectricity, thermomagnetic, thermomechanical, and galvanomagnetic effects, electrolytic transferance, liquid helium fountain effects,[8] and chemical reactions. The experimental tests for the validity of the Onsager relations have been reviewed extensively by Miller.[9] The linear theory for approach to equilibrium was developed further when Prigogine presented his studies on the so-called stationary states and proved an important theorem on entropy production rates, namely the minimum entropy production principle.[10–12]

From the point of view of pedagogy, clear explanations of the Onsager relations can be found in various textbooks (see Refs. 10, 11, 13, and 14, for examples; also see Ref. 15, for examples, dealing with thermal and electrical conduction in crystals and Ref. 16 for an example of electrical transport in solutions containing several electrolytes). For example, in Ref. 13, a statistical mechanics textbook designed for upper-level undergraduates and graduate students, Onsager relations are discussed in the last chapter in the context of fluctuations, correlation functions, and noise spectra. Although the discussion is excellent we feel that more concrete examples are warranted. Textbook examples with multiple (and coupled) variables are in short supply, and such coupled variables are necessary to illustrate the Onsager relations. Though the general thermodynamic proofs for the Onsager symmetry relations are compelling, it would still be instructive to show an explicit example in which the kinetic coefficients are calculated inside of a very specific model. Furthermore, it would be instructive to continue such an example problem by providing some of the key statistical functions such as the cross-correlation functions and the various spectral density functions that describe the fluctuations in the basic variables of the system.

Here, we present a very specific problem that involves transport of two variables—internal energy and particle number—in an effusing system. There is only one Onsager relation for this system and this is the relation we seek to investigate thoroughly. The goal here is quite direct: after reviewing the general thermodynamic approach and justification for the Onsager symmetry, we present a specific kinetic gas theory calculation that allows direct calculation of the Onsager coefficients.

We begin by setting up the Onsager analysis for approach to equilibrium, specific to the case of effusion of a single-species monatomic classical ideal gas. In Sec. II, we set up the basic equilibrium thermodynamics, which is used in Sec. III to define the conjugate forces which play an important role in restoring equilibrium. After defining, in Sec. IV, the Onsager **L** matrix that describes the nonequilibrium dynamics, we proceed, in Secs. V and VI, to use kinetic gas theory to explicitly calculate the matrix elements and verify the single Onsager symmetry. The basic steps for this solution are sketched out in Ref. 10. Here, we fill in the details and attempt to explain the physics carefully and avoid confusion. We follow this with example calculations, in Secs. VII and VIII, for dynamical approaches to equilibrium, which includes a careful discussion of the stationary states defined by Prigogine. Before concluding, we calculate the correlation functions (Sec. IX) and spectral density functions (Sec. X) for this system. The elementary level of treatment presented here makes this interesting result pedagogically useful for upper-level undergraduate level courses and graduate level courses in statistical thermodynamics.

II. ENTROPY CHANGE AS A QUADRATIC FORM

Consider two identical chambers, each with fixed volume V and containing a classical ideal gas of atoms of mass m (see Fig. 1). The total number of atoms is fixed at $2N_0$ and the total energy is fixed at $2U_0$. Before $t=0$ the two chambers are isolated, with the left chamber containing N_L atoms and the right chamber containing $N_R = 2N_0 - N_L$. We assume that the difference $\Delta N \equiv N_R - N_0$ is small ($\Delta N \ll N_0$), and likewise

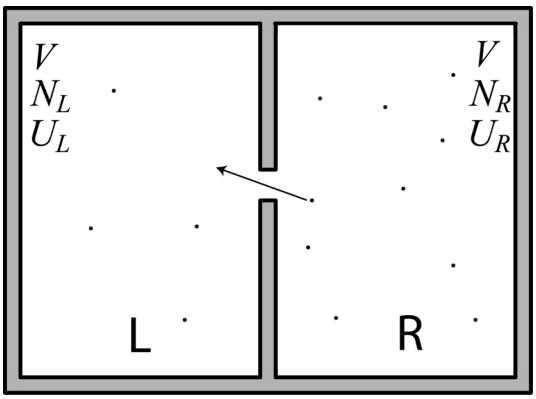

Fig. 1. Two identical chambers, each with volume V, labeled as left (L) and right (R). Between the chambers is a small hole opened at $t=0$ to allow for gas effusion.

$\Delta U \equiv U_R - U_0 \ll U_0$. After $t=0$, a small aperture is opened allowing atoms to move between the chambers. The equilibrium values for particle number and internal energy in each chamber are N_0 and U_0, respectively.

The entropy of a classical ideal gas in equilibrium is given by the Sackur-Tetrode equation[17]

$$S_0 = N_0 k_B \left\{ \ln\left[\frac{V}{N_0} \left(\frac{4\pi m U_0}{3h^2 N_0} \right)^{3/2} \right] + \frac{5}{2} \right\}, \tag{1}$$

where h is Planck's constant and k_B is Boltzmann's constant. In our system the total system entropy is twice this, in equilibrium. If $\Delta N \ll N_0$ particles and $\Delta U \ll U_0$ energy move into the left side, then the total entropy should be smaller. The expression for this total entropy is

$$\begin{aligned} \frac{S_T}{k_B} &= (N_0 + \Delta N) \\ &\times \left\{ \ln\left[\frac{V}{(N_0+\Delta N)^{5/2}} \left(\frac{4\pi m (U_0 + \Delta U)}{3h^2} \right)^{3/2} \right] + \frac{5}{2} \right\} \\ &+ (N_0 - \Delta N) \\ &\times \left\{ \ln\left[\frac{V}{(N_0-\Delta N)^{5/2}} \left(\frac{4\pi m (U_0 - \Delta U)}{3h^2} \right)^{3/2} \right] + \frac{5}{2} \right\}. \end{aligned} \tag{2}$$

Standard expansion techniques give $S_T = 2S_0 + \Delta S_T$, where

$$\frac{\Delta S_T}{k_B} = -\frac{3N_0 \Delta U^2}{2U_0^2} - \frac{5\Delta N^2}{2N_0} + \frac{3\Delta N \Delta U}{U_0}. \tag{3}$$

We now adopt some conventions of Ref. 10 and define $\Delta S \equiv \Delta S_T/2$, $a_1 \equiv \Delta U/U_0$, and $a_2 \equiv \Delta N/N_0$. The entropy change can then be written as a quadratic form

$$\Delta S = -\frac{1}{2}[g_{11}a_1^2 + g_{22}a_2^2 + 2g_{12}a_1 a_2]. \tag{4}$$

Comparing to Eq. (3) gives $g_{11} = 3N_0 k_B/2$, $g_{12} = g_{21} = -3k_B N_0/2$, and $g_{22} = 5k_B N_0/2$. These coefficients can be expressed as a matrix

$$\mathbf{G} = \frac{k_B N_0}{2} \begin{pmatrix} 3 & -3 \\ -3 & 5 \end{pmatrix}. \tag{5}$$

The determinant of $\mathbf{G}$, given by $\det G = 3k_B^2 N_0^2/2$, is never negative, as must be the case since the quadratic form in Eq. (4) must be non-positive definite in order to give maximum total entropy in equilibrium. The inverse of $\mathbf{G}$, given by

$$\mathbf{G}^{-1} = \frac{1}{3k_B N_0} \begin{pmatrix} 5 & 3 \\ 3 & 3 \end{pmatrix}, \tag{6}$$

will be useful below.

III. CONJUGATE FORCES

The expression in Eq. (4) for ΔS is useful for calculating the thermodynamic conjugate forces, which play a key role in restoring equilibrium. To understand the meaning of these conjugate forces, it is helpful first to think in general of thermodynamic conjugate variable pairs such as (P, V), (μ, N), etc. For the discrete system considered here, we might consider what variable would drive the system towards equilibrium if, for example, the particle number N is perturbed. This variable can be loosely thought of as a "force," though of course it may not have dimensions of force. This "force" would lead to a rate of change dN/dt, which we can think of as a "flux." Relating "fluxes" to "forces" is the essence of the approach taken by Onsager, Prigogine, de Groot, etc., in their descriptions of nonequilibrium dynamics.[3,10,11]

From our two variables a_i then, we evaluate the thermodynamic conjugate forces as $X_1 \equiv \partial(\Delta S)/\partial a_1$ and $X_2 \equiv \partial(\Delta S)/\partial a_2$. We note that these are not direct derivatives of the entropy as given by the Sackur-Tetrode equation (1). Rather, they are derivatives of the entropy difference ΔS. These derivatives work out to be

$$X_1 = -g_{11}a_1 - g_{12}a_2 = \frac{3}{2}k_B N_0[-\Delta U/U_0 + \Delta N/N_0], \tag{7}$$

$$X_2 = -g_{21}a_1 - g_{22}a_2 = \frac{3}{2}k_B N_0 \left[\Delta U/U_0 - \frac{5}{3}\Delta N/N_0 \right]. \tag{8}$$

Note that the conjugate forces are zero at equilibrium, analogous to a drag force that depends on velocity in a linear fashion. In vector format,

$$\vec{X} = -\mathbf{G}\vec{a}. \tag{9}$$

One would expect the force X_1 to be closely related to ΔT, the temperature difference between the two chambers. Similarly, X_2 should be closely related to $\Delta\mu$, the difference in chemical potential. To obtain these relations we proceed backwards. For a monatomic classical ideal gas, we have $T = 2U_0/(3N_0 k_B)$, so

$$\Delta T = \frac{\partial T}{\partial U}\Delta U + \frac{\partial T}{\partial N}\Delta N, \tag{10}$$

$$b_1 \equiv \frac{\Delta T}{T} = a_1 - a_2. \tag{11}$$

The chemical potential is given by

$$\mu = -\frac{2U_0}{3N_0}\ln\left[\frac{V}{N_0}\left(\frac{4\pi m U_0}{3N_0 h^2}\right)^{3/2}\right], \tag{12}$$

which implies

$$\Delta\mu = \frac{\partial\mu}{\partial U}\Delta U + \frac{\partial\mu}{\partial N}\Delta N, \tag{13}$$

$$\Delta\mu = \left[\frac{\mu}{U_0} - \frac{1}{N_0}\right]\Delta U + \left[-\frac{\mu}{N_0} + \frac{5U_0}{3N_0^2}\right]\Delta N, \tag{14}$$

$$b_2 \equiv \frac{N_0\Delta\mu}{U_0} = \left[\frac{N_0\mu}{U_0} - 1\right]a_1 - \left[\frac{N_0\mu}{U_0} - \frac{5}{3}\right]a_2. \tag{15}$$

The b_i variables are just as natural to use as the a_i variables and can be expressed in terms of the a_i variables using a transformation matrix $\mathbf{T}$:

$$\vec{b} = \mathbf{T}\vec{a} = \begin{pmatrix} 1 & -1 \\ N_0\mu/U_0 - 1 & -N_0\mu/U_0 - 5/3 \end{pmatrix}\vec{a}. \tag{16}$$

Using Eqs. (9) and (16), we note that $\vec{X} = -\mathbf{G}\mathbf{T}^{-1}\vec{b}$.

At this point, one could decide to use the variables b_i instead of a_i, or even combinations such as a_1 and b_2; this could be a valuable exercise. We could even choose to use ΔP as one of the two basic variables. Indeed, in his analysis de Groot uses the variables ΔT and ΔP.[10] Here, we elect to proceed with the simpler and more direct a_i variables and explain all the steps carefully, for pedagogic reasons.

A. Fluctuations and equilibrium averaging

All of the variables discussed so far are statistical in nature. One therefore proceeds to determine mean values for these variables, calculated using some averaging procedure from some probability distribution. One can also calculate higher moments of the probability distribution. In particular, the second moments are generally used to quantify the amount of fluctuation in the given variables. Here, we will use ensemble averaging, which will be denoted by angle brackets $\langle\cdots\rangle$; for example, $\langle a_i\rangle$ and $\langle X_i\rangle$. Performing the weighted ensemble averaging will involve considering states having total entropy values smaller than the equilibrium value. States with entropy values much smaller than the equilibrium value would be improbable. The weighting factor used in equilibrium ensemble averages is $\exp(\Delta S/k_B)$, which assumes the second law of thermodynamics.[10,13,14] The probability of a state lying in the intervals a_1 to $a_1 + da_1$ and a_2 to $a_2 + da_2$ is then

$$P\,da_1 da_2 = \frac{\exp(\Delta S/k_B)\,da_1 da_2}{\int\int \exp(\Delta S/k_B)\,da_1 da_2}. \tag{17}$$

This expression is properly normalized so that integration over all states gives unity. We can directly see that states with very large values of a_1 or a_2 will contribute very little to the sum. Given Eq. (4), we note that the moments of this probability distribution can be evaluated as Gaussian integrals. One readily verifies that $\langle a_i\rangle_0 = 0$ in equilibrium, where the subscript 0 denotes equilibrium averaging. Note that $\langle a_i\rangle$ may not be zero when the system is out of equilibrium. For the second moments, we note that $d\ln P/da_i = X_i/k_B$, so

$$\begin{aligned}\langle a_i X_j\rangle_0 &= \int_{-\infty}^{\infty}\int_{-\infty}^{\infty} a_i X_j P\,da_1 da_2 \\ &= k_B\int_{-\infty}^{\infty}\int_{-\infty}^{\infty} a_i\frac{d\ln P}{da_j}P\,da_1 da_2 \\ &= k_B\int_{-\infty}^{\infty}\int_{-\infty}^{\infty} a_i\frac{dP}{da_j}da_1 da_2,\end{aligned} \tag{18}$$

and integration by parts yields

$$\langle a_i X_j\rangle_0 = -k_B\int_{-\infty}^{\infty}\int_{-\infty}^{\infty}\delta_{ij}P\,da_1 da_2 = -k_B\delta_{ij}. \tag{19}$$

Specifically, $\langle a_1X_1\rangle_0 = \langle a_2X_2\rangle_0 = -k_B$ and $\langle a_1X_2\rangle_0 = \langle a_2X_1\rangle_0 = 0$. Use of Eqs. (6), (9), and (19) allows quick evaluation of the other second moments:

$$\langle X_i X_j\rangle_0 = -\sum_k g_{ik}a_k X_j = k_B g_{ij}, \tag{20}$$

$$\langle a_i a_j\rangle_0 = -\sum_k g_{ik}^{-1}X_k a_j = k_B g_{ij}^{-1}. \tag{21}$$

Explicitly, then,

$$\langle a_1^2\rangle_0 = \left\langle\frac{(\Delta U)^2}{U_0^2}\right\rangle_0 = \frac{5}{3N_0}, \tag{22}$$

$$\langle a_2^2\rangle_0 = \left\langle\frac{(\Delta N)^2}{N_0^2}\right\rangle_0 = \frac{1}{N_0}, \tag{23}$$

$$\langle a_1 a_2\rangle_0 = \left\langle\frac{\Delta U\Delta N}{U_0 N_0}\right\rangle_0 = \frac{1}{N_0}. \tag{24}$$

IV. APPROACH TO EQUILIBRIUM AND THE ONSAGER RELATIONS

For systems approaching equilibrium, our goal is to obtain a set of dynamical equations—differential equations involving time derivatives. When the deviations from equilibrium are small enough to allow linear equations, we can use the conjugate forces to write the desired equations in the following form:

$$\frac{da_1}{dt} \equiv \dot{a}_1 = L_{11}X_1 + L_{12}X_2, \tag{25}$$

$$\frac{da_2}{dt} \equiv \dot{a}_2 = L_{21}X_1 + L_{22}X_2. \tag{26}$$

The linearity of these equations means that the coefficients L_{ij} are all constant. It is helpful to compare to the single-variable example of ohmic conduction: $\dot{q} = GV$, where the potential difference V plays the role of conjugate force and the conductance G plays the role of the L coefficient. In

general, the coefficients L_{ij} have interesting properties. One such property is a consequence of the second law, which guarantees that the total system entropy production is never negative.[10] The consequence is that the diagonal elements L_{11} and L_{22} cannot be negative. The off-diagonal coefficients also have interesting symmetry properties, first recognized by Onsager. In the case of two variables, the Onsager symmetry relation is

$$L_{12} = L_{21}. \tag{27}$$

Derivations of Eqs. (25) and (26) can be found in Refs. 10, 13, and 14. Though these discussions vary, they all have in common the prominent use of the same Boltzmann weighting factor $\exp(\Delta S/k_B)$, as used above.

We point out that the time derivative must be coarse-grained. This means the time step Δt taken in the discrete version of the time derivative must be much larger than the characteristic time scale τ^* for the random force function that drives the fluctuations in the system. This time scale is generally a very fast microscopic quantity. In a gas, τ^* would be the mean time between collisions. In order to evaluate a meaningful derivative, we must smooth over time much longer than τ^*. The coarse-grained quantity will be denoted by an overbar:

$$\overline{\dot{a}_i}(t) \equiv \frac{1}{\Delta t}\int_t^{t+\Delta t} \langle \dot{a}_i(t')\rangle dt' = \frac{\langle a_i(t+\Delta t)\rangle - \langle a_i(t)\rangle}{\Delta t}, \tag{28}$$

where $\Delta t \gg \tau^*$. Substituting in Eqs. (25) and (26) gives

$$\frac{a_i(t+\Delta t) - a_i(t)}{\Delta t} = L_{i1}X_1 + L_{i2}X_2. \tag{29}$$

We can prove the Onsager relation, Eq. (27), by first multiplying both sides of Eq. (29) by $a_j(t)$ and then performing a time average over a section of time much longer than τ^*, which we denote by the braces $\{\}$:

$$\frac{\{\langle a_j(t)\rangle\langle a_i(t+\Delta t)\rangle\} - \{\langle a_j(t)\rangle\langle a_i(t)\rangle\}}{\Delta t} = L_{i1}\{\langle a_j(t)\rangle\langle X_1(t)\rangle\} + L_{i2}\{\langle\langle a_j(t)\rangle X_2(t)\rangle\}. \tag{30}$$

If, for the moment, we make all statistical averages equilibrium averages, then application of the ergodic theorem means that ensemble and time averages are the same so that $\{a_j(t)X_k(t)\} = \langle a_j(t)X_k(t)\rangle_0 = -k_B\delta_{jk}$, using Eq. (19). Setting $i=1, j=2$ in Eq. (29) gives

$$\langle a_2(t)a_1(t+\Delta t)\rangle_0 - \langle a_2(t)a_1(t)\rangle_0 = -k_B L_{12}\Delta t, \tag{31}$$

while setting $i=2, j=1$ gives

$$\langle a_1(t)a_2(t+\Delta t)\rangle_0 - \langle a_1(t)a_2(t)\rangle_0 = -k_B L_{21}\Delta t. \tag{32}$$

Invoking microscopic time-reversal symmetry, as we would expect during collisions between gas atoms, gives $\langle a_1(t)a_2(t+\Delta t)\rangle_0 = \langle a_1(t)a_2(t-\Delta t)\rangle_0$, which is the same as $\langle a_1(t+\Delta t)a_2(t)\rangle_0$ after making the substitution $t \to t+\Delta t$. Equation (32) then becomes

$$\langle a_1(t+\Delta t)a_2(t)\rangle_0 - \langle a_2(t)a_1(t)\rangle_0 = -k_B L_{21}\Delta t. \tag{33}$$

Comparing Eqs. (31) and (33), we see that both have the same left-hand sides, so we conclude that $L_{12} = L_{21}$. Thus, we have a general proof for this symmetry relation. This is the relation that we wish to verify explicitly in this work.

Such direct examples are not common. In fact, the only other one known to the author is one involving gas flow when the aperture is much larger than the mean free path. It is natural for students to have some doubts in accepting very general arguments. It is always preferable to follow these up with a concrete example, especially one with an exact solution. Here, we have such an exact solution from kinetic gas theory, and we do indeed confirm the Onsager symmetry relation in Sec. VI.

In order to streamline the notation, from here on the ensemble averaging brackets $\langle\cdots\rangle$ will be dropped for single moments and will be kept only for second moments and correlation functions. In vector format, Eqs. (25) and (26) can be written as

$$\dot{\vec{a}} = \mathbf{L}\vec{X}. \tag{34}$$

The matrix $\mathbf{L}$, like $\mathbf{G}$, is symmetric. Our goal is to explicitly determine the matrix $\mathbf{L}$ in a specific case and therefore verify the Onsager symmetry relation.

A. Stationary states and the principle of minimum entropy production

The conjugate force variables can be easily used to write down an expression for the rate of total entropy production:

$$\sigma_T \equiv \frac{dS_T}{dt} = X_1\dot{a}_1 + X_2\dot{a}_2 = L_{11}X_1^2 + L_{12}X_1X_2 + L_{21}X_1X_2 + L_{22}X_2^2. \tag{35}$$

In order to not violate the second law, this quadratic form must be non-negative definite. We note that even though the rates $\sigma_1 \equiv X_1\dot{a}_1$ and $\sigma_2 \equiv X_2\dot{a}_2$ may be conceptually helpful there is no guarantee that each is non-negative definite. Indeed, one of these rates could be negative while the other is positive (and the sum $\sigma_T = \sigma_1 + \sigma_2$ is non-negative).

Differentiating Eq. (35) with respect to X_1 and setting to zero gives $2L_{11}X_1 + L_{12}X_2 + L_{21}X_2 = 0$, which is the same as setting $\dot{a}_1 = 0$, after using the Onsager symmetry. The condition $\dot{a}_1 = 0$ defines what Prigogine referred to as a stationary state. Straightforward calculation shows that the total rate of entropy production is minimized in such a state. The basic idea is that for this stationary state, which we label as Type 1, X_2 is held fixed and X_1 is varied until σ_T is minimized. Substituting back into Eq. (35), we obtain $\sigma_T = \sigma_2 = L_{21}X_1X_2 + L_{22}X_2^2 = [1 - L_{12}^2/(L_{11}L_{22})]L_{22}X_2^2$. We note that this rate is indeed smaller than $L_{22}X_2^2$, which is the rate that would be obtained if variable X_1 was set to zero. In our example, there will be two stationary states, with the other, Type 2, defined by setting $\dot{a}_2 = 0$. For Type 2 states, $\sigma_2 = 0$.

V. EFFUSION ANALYSIS

The Onsager coefficients L_{ij} relate thermodynamic forces X_i that are calculated using equilibrium thermodynamics, to the thermodynamic fluxes $\dot{a}_i$. We calculate these fluxes using non-equilibrium effusion analysis, which will allow us to explicitly calculate the L_{ij} coefficients. An excellent analysis of the effusion process can be found in Ref. 13, Chapter 7.

Essentially, the process of particle transfer is random diffusion through the aperture, which is assumed to be much smaller than the mean free path of the gas atoms. This process is also known as Knudsen flow. We briefly review the analysis that applies standard kinetic theory for a classical ideal gas. The gas statistics are described by the Maxwell velocity distribution,

$$f(v)\,d^3\vec{v} = n\left(\frac{m}{2\pi k_B T}\right)^{3/2} e^{-mv^2/(2k_B T)}\,d^3\vec{v}. \tag{36}$$

The flux Φ_N of particles from the left side to the right side is obtained by integrating the velocity distribution over a hemisphere (solid angle of 2π steradians) with the z-axis aligned perpendicular to the aperture:

$$\Phi_N = \int_{v_z>0} d^3\vec{v} f(v) v_z = \int_{v_z>0} dv\ d\Omega\ v^2 f(v) v\cos\theta. \tag{37}$$

In terms of the polar angle θ and azimuthal angle ϕ, we have

$$\begin{aligned}\Phi_N &= \int_0^\infty dv \int_0^{\pi/2} d\theta \int_0^{2\pi} d\phi\ v^3 \sin\theta\cos\theta\ f(v)\\ &= \pi\int_0^\infty dv\ v^3\ f(v)\\ &= \frac{1}{4}n\bar{v} = \frac{P}{\sqrt{2\pi m k_B T}} = \frac{\sqrt{N_0 U_0}}{V\sqrt{3\pi m}},\end{aligned} \tag{38}$$

where we have made use of the ideal gas equation $PV = N_0 k_B T = 2U_0/3$, and $\bar{v}$ is the mean particle speed. We note that the $\sqrt{m}$ factor in the denominator implies Graham's law. For an aperture area of πr^2, the time rate of particle increase is

$$\begin{aligned}\dot{N} &= -\pi r^2 \Delta\Phi_N = -\pi r^2\left[\frac{\partial\Phi_N}{\partial U}\Delta U + \frac{\partial\Phi_N}{\partial N}\Delta N\right]\\ &= -\frac{1}{2}\pi r^2 \Phi_N[a_1 + a_2].\end{aligned} \tag{39}$$

Note that the use of just first derivatives implies a purely linear result, which is fully consistent with the linear thermodynamic approach summarized by Eq. (34).

A. Energy flux

Since each effusing particle carries along an energy $mv^2/2$, the energy flux from the left side to the right side is

$$\begin{aligned}\Phi_U &= \int_{v_z>0} d^3\vec{v} f(v)\frac{1}{2}mv^2 v_z = \frac{\pi m}{2}\int_0^\infty dv\, v^5 f(v)\\ &= 2k_B T\Phi_N.\end{aligned} \tag{40}$$

We note that the ratio Φ_U/Φ_N is not the mean particle energy $3k_BT/2$. Each of the two spatial components parallel to the aperture contributes $k_BT/2$ of energy, but the perpendicular component contributes twice as much, giving $2k_BT$. For effusion, the perpendicular component is favored and has greater weight in the flux integral. Using $U_0 = 3N_0k_BT/2$ and eliminating Φ_N, we have

$$\Phi_U = \frac{4U_0}{3N_0}\Phi_N = \frac{4U_0^{3/2}N_0^{-1/2}}{3V\sqrt{3\pi m}}. \tag{41}$$

The rate of change of internal energy is given by

$$\begin{aligned}\dot{U} &= -\pi r^2\Delta\Phi_U = -\pi r^2\left[\frac{\partial\Phi_U}{\partial U}\Delta U + \frac{\partial\Phi_U}{\partial N}\Delta N\right]\\ &= -\frac{1}{2}\pi r^2\Phi_U[3a_1 - a_2].\end{aligned} \tag{42}$$

Dividing both sides by U_0 gives

$$\dot{a}_1 = -\left(\frac{\pi r^2\Phi_N}{N_0}\right)\frac{2}{3}[3a_1 - a_2]. \tag{43}$$

In matrix form, the effusion dynamics is described by

$$\dot{\vec{a}} = \mathbf{A}\vec{a}\ , \tag{44}$$

where

$$\mathbf{A} = -\left(\frac{\pi r^2\Phi_N}{N_0}\right)\begin{pmatrix}2 & -2/3\\ 1/2 & 1/2\end{pmatrix}. \tag{45}$$

At this point, we define the characteristic timescale for this system as

$$\tau_0 = \frac{N_0}{\pi r^2\Phi_N} = \frac{V}{\pi r^2}\sqrt{\frac{3\pi m N_0}{U_0}}. \tag{46}$$

We note that when comparing the diagonal matrix elements, A_{11} being greater in magnitude than A_{22}, that the energy transfer process is inherently faster than the particle transfer. This will reveal itself below in the diagonalization of this matrix.

VI. CONNECTING THERMODYNAMICS TO KINETICS

Summarizing our results so far, we have one matrix $\mathbf{G}$ that relates X_i to a_i using an ideal gas statistical thermodynamic model; another matrix $\mathbf{L}$ that relates $\dot{a}_i$ to X_i using general thermodynamical arguments; and a final matrix $\mathbf{A}$ that relates $\dot{a}_i$ to a_i using the kinetic theory of gases. All of these approaches produce results at linear order. Comparing Eqs. (9), (34), and (44), we see that $\mathbf{A} = -\mathbf{LG}$. This will allow us to directly calculate the $\mathbf{L}$ matrix so we can verify the Onsager relation $L_{12} = L_{21}$. Solving for $\mathbf{L}$ then given

$$\mathbf{L} = -\mathbf{A}\mathbf{G}^{-1}, \tag{47}$$

so that

$$\mathbf{L} = \left(\frac{1}{3k_BN_0\tau_0}\right)\begin{pmatrix}8 & 4\\ 4 & 3\end{pmatrix}. \tag{48}$$

We do indeed recover the expected result:

$$L_{12} = L_{21} = \frac{4}{3k_BN_0\tau_0}. \tag{49}$$

This is the main result we were aiming for. We also readily verify that the diagonal elements of the $\mathbf{L}$ matrix are

non-negative and that the determinant of **L** is positive, as demanded to ensure thermodynamic stability. In particular, $L_{12}^2/(L_{11}L_{22}) = 2/3$ and $1 - L_{12}^2/(L_{11}L_{22}) = 1/3$. In what follows we strive to elucidate some of the general features of nonequilibrium thermodynamics (i.e., not thermostatics) using this specific effusion example.

VII. DIAGONALIZATION OF A: TWO TIMESCALES

Solving the eigenvalue equation for the matrix **A** will allow us to solve Eq. (44) and obtain solutions for initial value problems, as well as for the various correlation functions. From here on we express **A** in units of $\pi r^2 \Phi_N/N_0 = 1/\tau_0$, **L** in units of $\pi r^2 \Phi_N/(3k_B N_0^2)$, and **G** in units of $k_B N_0/2$.

The characteristic polynomial is $4/3 + 5\lambda\tau_0/2 + (\lambda\tau_0)^2$, which produces two real, negative eigenvalues. We note that the dynamical equation can also be expressed as $\dot{\vec{X}} = \mathbf{GAG^{-1}}\vec{X}$, and that this produces the same eigenvalues. The smaller-magnitude eigenvalue, labeled λ_s, results in slower dynamics and is given by $\lambda_s\tau_0 = -5/4 + \sqrt{33}/12 \approx -0.77129$. Similarly, the fast eigenvalue is given by $\lambda_f\tau_0 = -5/4 - \sqrt{33}/12 \approx -1.72871$, approximately 2.241 times larger.

Because the matrix **A** is not symmetric, the eigenvectors are not orthogonal. Explicitly:

$$\vec{v}_f = \begin{pmatrix} (9+\sqrt{33})/6 \\ 1 \end{pmatrix} \approx \begin{pmatrix} 2.45743 \\ 1 \end{pmatrix}, \tag{50}$$

$$\vec{v}_s = \begin{pmatrix} (9-\sqrt{33})/6 \\ 1 \end{pmatrix} \approx \begin{pmatrix} 0.542573 \\ 1 \end{pmatrix}, \tag{51}$$

$$\vec{v}_f(t) \approx \begin{pmatrix} 2.45743 \\ 1 \end{pmatrix} e^{-1.72871 t/\tau_0}, \tag{52}$$

$$\vec{v}_s(t) \approx \begin{pmatrix} 0.542573 \\ 1 \end{pmatrix} e^{-0.77129 t/\tau_0}. \tag{53}$$

The vectors $\vec{v}_f(t)$ and $\vec{v}_s(t)$ are independent solutions to Eq. (44). We note that $\vec{v}_f$ has more weight in the a_1 variable than in a_2. Likewise, the slow eigenvector has more weight in a_2 than in a_1. Even though these vectors are both mixtures, we conclude that for this system the energy transfer is a faster process than straight particle transfer.

If the system is initially prepared in a state so that the initial values a_1 and a_2 form a vector $\vec{a}$ proportional to $\vec{v}_f$, then both ΔU and ΔN will decay with only one timescale (the fast one). This is illustrated in Fig. 2 (solid curves), along with the solutions where $\vec{a}(0)$ is proportional to the slow eigenvector (dashed curves). In order to assist with solution of initial value problems, we define a fundamental matrix $\mathbf{\Psi}$ using the two eigenvectors as columns

$$\mathbf{\Psi(t)} = (\vec{v}_f(t) \quad \vec{v}_s(t)) = \begin{pmatrix} 2.45743\, e^{\lambda_f t} & 0.542573\, e^{\lambda_s t} \\ e^{\lambda_f t} & e^{\lambda_s t} \end{pmatrix}. \tag{54}$$

The same eigenvectors can be used to write general solutions to the initial value problem, given $a_1(0)$ and $a_2(0)$, so that

$$\vec{a}(t) = \mathbf{\Phi}(t)\vec{a}(0), \tag{55}$$

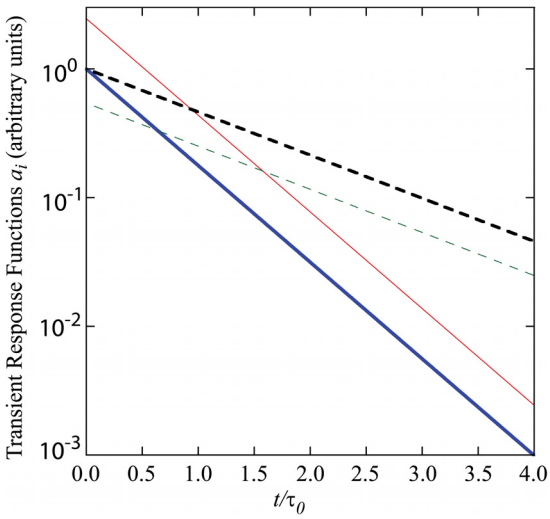

Fig. 2. Semi-log plots of transient response functions for the effusing system when initially prepared in either of the two eigenvectors. Solid (dashed) curves correspond to the fast (slow) eigenstate, with thin curves plotting $a_1(t)$ and thick curves plotting $a_2(t)$. The time scale is in units of τ_0 as given in Eq. (46).

where

$$\mathbf{\Phi}(t) \equiv \mathbf{\Psi}(t)\mathbf{\Psi}^{-1}(0) = \begin{pmatrix} 2.45743\, e^{\lambda_f t} & 0.542573\, e^{\lambda_s t} \\ e^{\lambda_f t} & e^{\lambda_s t} \end{pmatrix} \times \begin{pmatrix} 0.522233 & -0.28335 \\ -0.522233 & 1.28335 \end{pmatrix} \tag{56}$$

is the special fundamental matrix, which equals the identity matrix at $t = 0$.[18] Explicitly, the elements of $\mathbf{\Phi}$ are

$$\mathbf{\Phi}_{11}(t) = 1.28335\, e^{\lambda_f t} - 0.28335\, e^{\lambda_s t}, \tag{57}$$

$$\mathbf{\Phi}_{12}(t) = -0.69631\, e^{\lambda_f t} + 0.69631\, e^{\lambda_s t}, \tag{58}$$

$$\mathbf{\Phi}_{21}(t) = 0.522233\, e^{\lambda_f t} - 0.522233\, e^{\lambda_s t}, \tag{59}$$

$$\mathbf{\Phi}_{22}(t) = -0.28335\, e^{\lambda_f t} + 1.28335\, e^{\lambda_s t}, \tag{60}$$

and the components of Eq. (55) are

$$\begin{aligned} a_1(t) &= \mathbf{\Phi_{11}}(t)\, a_1(0) + \mathbf{\Phi_{12}}(t)\, a_2(0) \\ &= [1.28335\, e^{\lambda_f t} - 0.28335\, e^{\lambda_s t}]a_1(0) \\ &\quad + [-0.69631\, e^{\lambda_f t} + 0.69631\, e^{\lambda_s t}]a_2(0), \end{aligned} \tag{61}$$

$$\begin{aligned} a_2(t) &= \mathbf{\Phi_{21}}(t)\, a_1(0) + \mathbf{\Phi_{22}}(t)\, a_2(0) \\ &= [0.522233\, e^{\lambda_f t} - 0.522233\, e^{\lambda_s t}]a_1(0) \\ &\quad + [-0.28335\, e^{\lambda_f t} + 1.28335\, e^{\lambda_s t}]a_2(0). \end{aligned} \tag{62}$$

VIII. INITIAL VALUE EXAMPLE PROBLEMS

Below, we consider three interesting examples, all of which involve time evolution involving the two time scales. The predictions from these three examples could be tested experimentally, using standard pressure gauges, pumps, and

vacuum fittings.[19] Preferably, one would have two identical vacuum chambers each filled to specified pressures with a monatomic gas, such as argon, and equipped with valves to isolate each chamber after filling. The aperture connecting the two chambers would be constructed using a precision variable leak valve, as commonly used in surface science studies.[20]

A. Problem 1: $\Delta N = 0$ initially

With $a_2(0) = 0$ we substitute $\vec{a}(0) = (1, 0)$ into Eq. (55); the solutions are plotted in Fig. 3. Physically this system could be set up by making sure both chambers start with the same number of atoms. Before $t = 0$ the right chamber is warmed up relative to the left chamber (aperture closed). When the aperture is opened at $t = 0$, there will be a net flow of particles from right to left (so $\dot{a}_2 < 0$) because the particles on the right have on average higher speeds. This takes ΔN away from its equilibrium value of zero. These effusing atoms carry energy, so a_1 decreases (rapidly). At some point ΔN gets large enough, and ΔU gets small enough, that we reach a stationary state where $\dot{a}_2$ becomes zero. From Eqs. (44) and (45), we see that this stationary state occurs when $a_1 = -a_2$. The stationary state lasts only momentarily, after which a_1, the energy variable, actually overshoots the equilibrium value. This overshoot is consistent with our assertion earlier that the energy transfer is fast compared to pure particle transfer. Soon after the overshoot, the system achieves a second stationary state, Type 1 this time, where $a_2 = 3a_1$. A negative value of $a_1 = -0.024$ is achieved at $t = 2.40$. Afterwards, both variables approach equilibrium values (mostly at the slower timescale).

We see in Fig. 3 that the two conjugate forces are both monotonic functions of time. In order to better understand these forces, it helps to look at the entropy production, which is plotted in Fig. 4. The rate σ_1 begins with positive values, as one might expect, since the variable a_1 was set away from zero initially. The inter-variable coupling causes a_2 to get

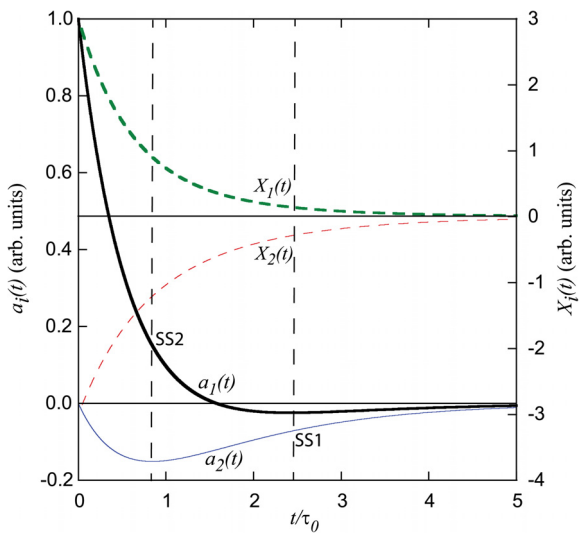

Fig. 3. Transient response functions with initial condition $a_2(0) = 0$. Solid curves represent the variables a_1 (thick) and a_2 (thin), while dashed curves represent X_1 (thick) and X_2 (thin). In this case, the solutions exhibit two stationary states: a Type-2 state at $t = 0.84$ where $a_2 = -a_1$, and a Type-1 state at $t = 2.40$ where $a_2 = 3a_1$. The time scale is in units of τ_0 as given in Eq. (46).

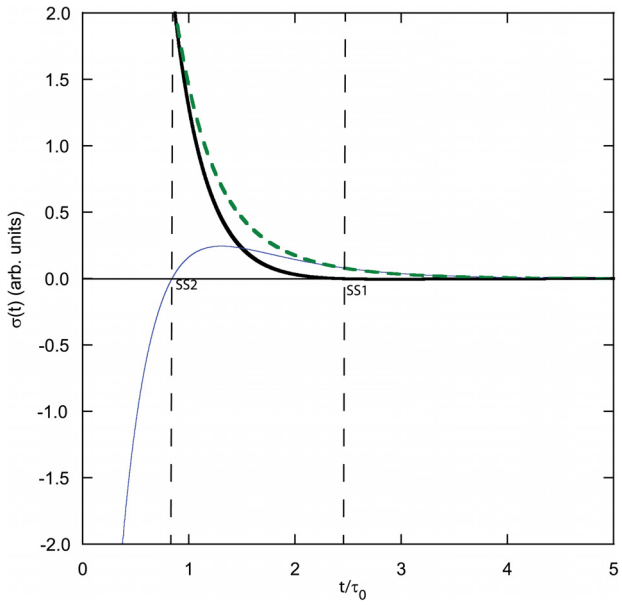

Fig. 4. Entropy production rates with initial condition $a_2(0) = 0$. Thick (thin) solid curves represent σ_1 (σ_2), while the total rate of entropy production is plotted as a dashed curve. Though it is difficult to make out, the thick solid curve for σ_1 does become negative after ≈ 2.40 s (SS1) and stays negative after that. The time scale is in units of τ_0 as given in Eq. (46).

pushed away from zero. Focusing on variable 2 only, the partial entropy decreases (see the thin solid curve). This would seem to make sense: for a single-variable system entropy is maximized at equilibrium, so pushing the system away from equilibrium would leave it with less entropy. However, here the two variables are coupled so we must be careful, as we will see in the next problem. There is no violation of the second law because the total entropy (dashed curve) continues to increase. We note that each chamber contributes equally to this total rate of entropy production. The rate σ_2 remains negative until the Type 2 stationary state is attained; after that $\sigma_2 > 0$. At $t \approx 2.40$ s, the Type 1 stationary state is attained. Subsequently, the entropy associated with variable 1 decreases due to the overshoot of a_1. Thus, we have the interesting result that there are times during which each partial entropy production rate (for each variable) is negative.

B. Problem 2: $\Delta U = 0$ initially

If we set the two chambers to initially contain the same amount of energy and make the right side contain more particles than the left side, then this situation can be described by the initial condition $a_1(0) = 0$. The solutions for $a_1(t)$ and $a_2(t)$ for this scenario are shown in Fig. 5. We see that the energy and particle number variables are again coupled. The particle number variable a_2 responds by approaching equilibrium monotonically. In order to satisfy our initial conditions, the temperature of the left chamber must start off higher than the right one. This results in energy flow towards the right chamber. There are particles flowing in both directions with more are moving from right to left, but the back-flowing particles each carry more energy making the net energy flow in the direction opposite to the net particle flow. This is the physical understanding for the sign of the A_{12} matrix component in Eq. (45). A Type-1 stationary state is achieved at $t = 0.84\tau_0$. Again, we see the presence of the two distinct time scales. Variable a_1 responds quickly at first, but subsequently, both

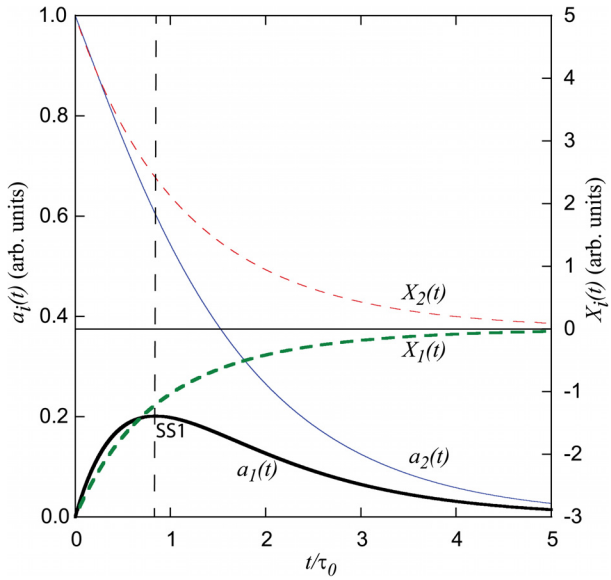

Fig. 5. Transient response functions with initial condition $a_1(0)=0$. Solid curves represent the variables a_1 (thick) and a_2 (thin), while dashed curves represent X_1 (thick) and X_2 (thin). The solutions exhibit a Type-1 stationary state at $t\approx 0.84$ where $a_2=3a_1$. The time scale is in units of τ_0 as given in Eq. (46).

variables decay to equilibrium at the slower timescale, reminiscent of a highly over-damped harmonic oscillator.

We point out some interesting physics pertaining to entropy production in this problem. Even though in this case variable a_1 gets pushed away from equilibrium immediately after $t=0$, the entropy production σ_1 is actually positive (see Fig. 6), in contrast to what happened to variable a_2 in Problem 1 above. One has to be careful and look at the signs of X_1 and $\dot{a}_1$ before deciding whether σ_1 is positive or negative. One also has to always remember that the two variables a_1 and a_2 are coupled. After passing $t=0.84\tau_0$, the rate σ_1 becomes negative and stays negative for all later times (with $\sigma_T>0$ throughout).

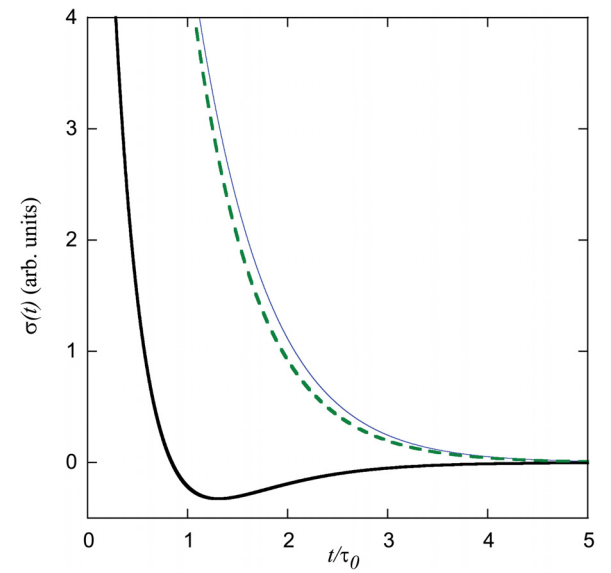

Fig. 6. Entropy production rates with initial condition $a_1(0)=0$. Thick (thin) solid curves represent σ_1 (σ_2), while the total rate of entropy production is plotted as a dashed curve. The time scale is in units of τ_0 as given in Eq. (46).

C. Problem 3: $\Delta T=0$, $\Delta N\neq 0$ initially

We consider one last case where before opening the aperture, both chambers are held at the same temperature, but the right chamber is held at higher pressure. This makes $\Delta N(0)>0$ as well as $\Delta U(0)>0$. The precise initial ratio of a_1 to a_2 is determined by differentiating $U=3Nk_BT/2$:

$$dU=\frac{3}{2}Nk_BdT+\frac{3}{2}k_BTdN. \tag{63}$$

With dT set to zero, we obtain

$$a_1(0)=\frac{\Delta U}{U}=\frac{\Delta N}{N}=a_2(0). \tag{64}$$

Figure 7 shows the results when the initial state vector $\vec{a}(0)$ is set to (1,1). We see the energy variable responding more quickly at first, as expected from the above discussion. Though both variables decay monotonically, we clearly see the presence of two timescales. We note that one might be tempted to solve this initial value problem with just one time scale, using an approach focused on particle transfer and ignoring energy transfer. The time scale would be $2\tau_0$, obtained from the 2, 2 element of the matrix in Eq. (45). As we have shown, however, the variables ΔN and ΔU are coupled, which means it is incorrect to ignore the effusion of energy. The actual approach to equilibrium is substantially faster than for the incorrect solution (see the thin short-dash curve for the incorrect plot of a_{INC}). These problems are tricky! See Ref. 13, Problem 7.28, and the solution in Ref. 21 for an example of precisely this error. Even though the solutions for a_1 and a_2 seem straightforward, we see in Fig. 8 that the rate of entropy production for a_1 is never positive for this solution.

D. Assessment of the stationary state concept

After analyzing three examples of stationary states, we must question their usefulness in the context of this effusion problem. These states are supposed to be helpful in regards to Prigogine's minimum entropy production principle. To

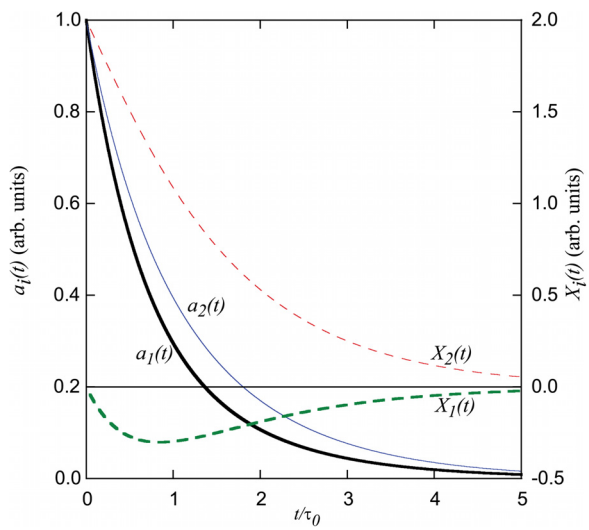

Fig. 7. Transient response functions with initial condition $a_1(0)=a_2(0)$. Solid curves represent the variables a_1 (thick) and a_2 (thin), while dashed curves represent X_1 (thick) and X_2 (thin). No stationary states are found in these solutions. The time scale is in units of τ_0 as given in Eq. (46).

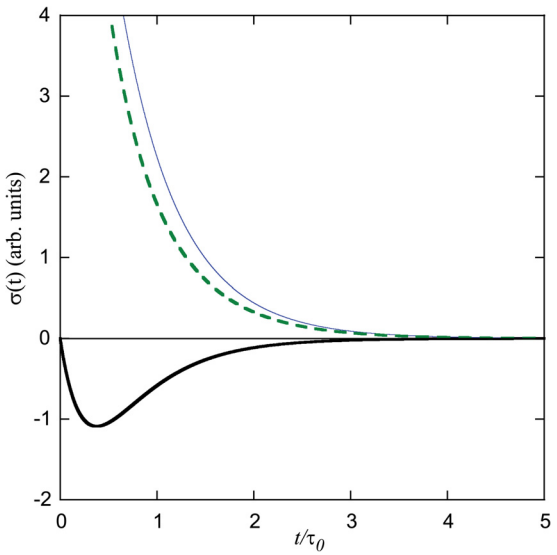

Fig. 8. Entropy production rates with initial condition $a_1(0) = a_2(0)$. Thick (thin) solid curves represent σ_1 (σ_2), while the total rate of entropy production is plotted as a dashed curve. The time scale is in units of τ_0 as given in Eq. (46).

reiterate, one holds one X variable constant and varies the other until σ_T is minimized. However, this does not apply in these examples because both X variables vary with time. One simply cannot hold X_1 constant and allow X_2 to vary (or vice-versa). The precise condition for a stationary state holds only momentarily, and in this sense the description "stationary" does not seem apt. It is true that at these moments in time, one of the partial rates of entropy production σ_i is zero, and the slope of $a_i(t)$ vs. t is zero. However, nothing else seems to be special about these stationary states. Certainly, the total rate of entropy production $\sigma_T(t)$ is not minimized with respect to time at these points and does not seem to display any interesting behavior (with respect to time) at these points.

We don't rule out the usefulness of the stationary state concept in general. In particular, for a two-variable system, we propose that the concept may be quite helpful in the case where the two time scales (from the diagonalization of **A**) are very disparate, i.e., one very slow and one very fast. If the initial conditions set the slow variable away from equilibrium with the fast one initially having a value of zero, then the fast variable would respond quickly at first and would (quickly) attain an almost stationary nonzero value for a long time. As far as the fast variable is concerned this quasi-stationary state would be sustained for a long time. In this case, a sustained condition of minimal entropy production should be interesting, and identifying the quasi-stationary states would be useful towards better understanding the system.

Returning to our effusing system, we note that the ratio of the two time scales is not adjustable, having the fixed value of 2.241. Thus, the stationary state concept is not worth the trouble for this work, and quite frankly, may create some confusion by having a misleading name. Before moving on we note that Prigogine's principle of minimum entropy production remains controversial in the literature, with maximum entropy production principles also vying for prominence. For a recent account of this active area of research, see the interview of Swenson in Ref. 22 and references within.

IX. CORRELATION FUNCTIONS

We can also use the special fundamental matrix to determine correlation functions. These basic statistical functions are useful in describing how a variable reacts to a stimulus that pushes the system slightly away from equilibrium (such as a significantly large, and rare, fluctuation). They can also be used to quantify the amount of fluctuation in a variable. For shorthand, we define

$$K_{a_i a_j}(s) \equiv \langle a_i(t+s) a_j(t) \rangle_0. \tag{65}$$

That the correlation functions are independent of t is a result of the ensemble averaging being over equilibrium states only. Using the same arguments (invoking time reversal symmetry) as we did above when proving $L_{12} = L_{21}$, we can show that $K_{a_i a_j}(-s) = K_{a_i a_j}(s)$ and $K_{a_i a_j}(s) = K_{a_j a_i}(s)$. Thus, the correlation functions $K_{a_i a_i}(s)$ are even in s and the cross-correlation matrix is symmetric.

In order to calculate these correlation functions, we begin by rewriting Eq. (44) as

$$\begin{pmatrix} \dot{a}_1(t) \\ \dot{a}_2(t) \end{pmatrix} = -\left(\frac{\pi r^2 \Phi_N}{6N_0}\right) \begin{pmatrix} 12 & -4 \\ 3 & 3 \end{pmatrix} \begin{pmatrix} a_1(t) \\ a_2(t) \end{pmatrix}. \tag{66}$$

Next, we follow a procedure similar to that found in Ref. 13, p. 576, where a single-variable system is treated. We adapt that procedure to the two-variable case here. We multiply both sides of Eq. (66) by $a_1(0)$ and then perform equilibrium ensemble averaging. We find that Eq. (66) holds for the correlation functions $\langle a_1(t) a_1(0) \rangle_0$ and $\langle a_2(t) a_1(0) \rangle_0$ as well. Recalling that the special fundamental matrix is used to solve initial value problems, Eq. (55) gets modified to become

$$\begin{aligned} \begin{pmatrix} \langle a_1(s) a_1(0) \rangle_0 \\ \langle a_2(s) a_1(0) \rangle_0 \end{pmatrix} &= \mathbf{\Phi}(s) \begin{pmatrix} \langle a_1(0) a_1(0) \rangle_0 \\ \langle a_1(0) a_2(0) \rangle_0 \end{pmatrix} \\ &= \mathbf{\Phi}(s) \begin{pmatrix} 5/(3N_0) \\ 1/N_0 \end{pmatrix}, \end{aligned} \tag{67}$$

valid for $s \geq 0$. Using Eqs. (22) and (24) then gives

$$\begin{pmatrix} K_{a_1 a_1}(s) \\ K_{a_2 a_1}(s) \end{pmatrix} = \mathbf{\Phi}(s) \begin{pmatrix} 5/(3N_0) \\ 1/N_0 \end{pmatrix}, \tag{68}$$

and similarly

$$\begin{pmatrix} K_{a_1 a_2}(s) \\ K_{a_2 a_2}(s) \end{pmatrix} = \begin{pmatrix} \langle a_1(s) a_2(0) \rangle_0 \\ \langle a_2(s) a_2(0) \rangle_0 \end{pmatrix} = \mathbf{\Phi}(s) \begin{pmatrix} 1/N_0 \\ 1/N_0 \end{pmatrix}. \tag{69}$$

Setting $s = 0$ gives the following important results:

$$\langle a_1(0) a_1(0) \rangle_0 \equiv \langle a_1^2 \rangle_0 = K_{a1a1}(0) = \frac{5}{3N_0}, \tag{70}$$

$$\langle a_1 a_2 \rangle_0 = \langle a_2 a_1 \rangle_0 = K_{a1a2}(0) = \frac{1}{N_0}, \tag{71}$$

$$\langle a_2^2 \rangle_0 = K_{a2a2}(0) = \frac{1}{N_0}. \tag{72}$$

The root-mean-square values of a_1 and a_2 are given by

$$a_{1\text{rms}} \equiv \sqrt{\langle a_1^2\rangle_0} = \sqrt{\frac{5}{3N_0}}, \tag{73}$$

$$a_{2\text{rms}} \equiv \sqrt{\langle a_2^2\rangle_0} = \frac{1}{\sqrt{N_0}}. \tag{74}$$

Thus, we can quantify the total amount of fluctuation in our variables. We also verify that these rms quantities scale as $N_0^{-1/2}$, so that in the thermodynamic limit ($N_0 \to \infty$) relative fluctuations disappear.

Returning to the case $s > 0$, if we combine Eq. (69) with Eqs. (61) and (62) we obtain

$$\begin{aligned} K_{a_1a_1}(s) &= \mathbf{\Phi}_{11}(t)\frac{5}{3N_0} + \mathbf{\Phi}_{12}(s)\frac{1}{N_0} \\ &= [1.28335\, e^{\lambda_f s} - 0.28335\, e^{\lambda_s s}]\frac{5}{3N_0} \\ &\quad + [-0.69631\, e^{\lambda_f s} + 0.69631\, e^{\lambda_s s}]\frac{1}{N_0} \\ &= 1.44261\frac{e^{\lambda_f s}}{N_0} + 0.22406\frac{e^{\lambda_s s}}{N_0}; \end{aligned} \tag{75}$$

$$\begin{aligned} K_{a_1a_2}(s) &= \mathbf{\Phi}_{11}(t)\frac{1}{N_0} + \mathbf{\Phi}_{12}(s)\frac{1}{N_0} \\ &= [1.28335\, e^{\lambda_f s} - 0.28335\, e^{\lambda_s s}]\frac{1}{N_0} \\ &\quad + [-0.69631\, e^{\lambda_f s} + 0.69631\, e^{\lambda_s s}]\frac{1}{N_0} \\ &= 0.58704\frac{e^{\lambda_f s}}{N_0} + 0.41296\frac{e^{\lambda_s s}}{N_0}; \end{aligned} \tag{76}$$

$$\begin{aligned} K_{a_2a_1}(s) &= \mathbf{\Phi}_{21}(t)\frac{5}{3N_0} + \mathbf{\Phi}_{22}(s)\frac{1}{N_0} \\ &= [0.522233\, e^{\lambda_f s} - 0.522233\, e^{\lambda_s s}]\frac{5}{3N_0} \\ &\quad + [-0.28335\ e^{\lambda_f s} + 1.28335 e^{\lambda_s s}]\frac{1}{N_0} \\ &= 0.58704\frac{e^{\lambda_f s}}{N_0} + 0.41296\frac{e^{\lambda_s s}}{N_0} = K_{a_1a_2}(s); \end{aligned} \tag{77}$$

$$\begin{aligned} K_{a_2a_2}(s) &= \mathbf{\Phi}_{21}(t)\frac{1}{N_0} + \mathbf{\Phi}_{22}(s)\frac{1}{N_0} \\ &= [0.522233\, e^{\lambda_f s} - 0.522233\, e^{\lambda_s s}]\frac{1}{N_0} \\ &\quad + [-0.28335\, e^{\lambda_f s} + 1.28335\, e^{\lambda_s s}]\frac{1}{N_0} \\ &= 0.23888\frac{e^{\lambda_f s}}{N_0} + 0.76112\frac{e^{\lambda_s s}}{N_0}. \end{aligned} \tag{78}$$

The correlation functions are easily calculated numerically and are displayed in Fig. 9. We have also verified the expected result that $\langle a_2(t)a_1(0)\rangle_0 = \langle a_1(t)a_2(0)\rangle_0$. Knowledge of correlation functions can be used to obtain noise spectra for variables such as pressure, chemical potential, etc., using Fourier transformation.

X. FOURIER ANALYSIS

The Fourier transforms of the correlation functions are given by

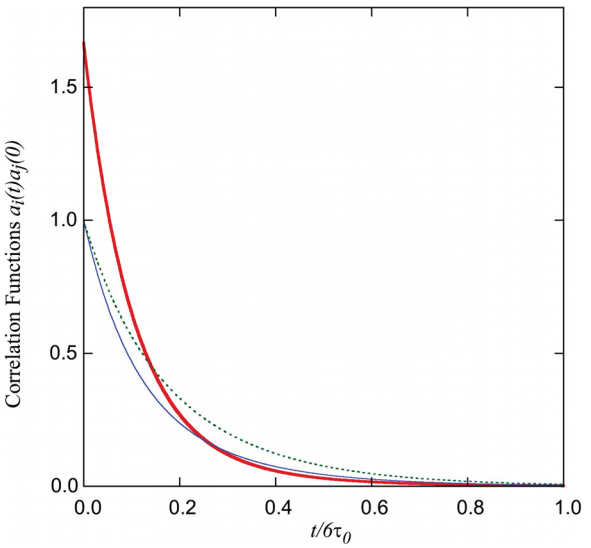

Fig. 9. Correlation functions $\langle a_1(t)a_1(0)\rangle_0$ (thick solid curve), $\langle a_2(t)a_1(0)\rangle_0$ (thin solid curve), and $\langle a_2(t)a_2(0)\rangle_0$ (dashed curve). Apart from being normalized by N_0, these functions are presented on actual scales. The time scale is in units of $6\tau_0$ with τ_0 given in Eq. (46).

$$J_{ij}(\omega) \equiv \frac{1}{2\pi}\int_{-\infty}^{\infty} K_{a_ia_j}(s)\, e^{-i\omega s} ds, \tag{79}$$

with inverse transforms

$$K_{a_ia_j}(s) = \int_{-\infty}^{\infty} J_{ij}(\omega)\, e^{i\omega s} d\omega. \tag{80}$$

These Wiener-Khintchine relations relate the correlation functions to the *spectral densities* J_{ij}. Making use of the relations $K^*_{a_ia_j}(s) = K_{a_ia_j}(s)$ (real functions) and $K_{a_ia_j}(-s) = K_{a_ia_j}(s)$ gives the following relations for the spectral densities:

$$J^*_{ij}(\omega) = J_{ij}(\omega), \tag{81}$$

$$J_{ij}(-\omega) = J_{ij}(\omega); \tag{82}$$

i.e., these spectral density functions are also real-valued and even functions of ω. It suffices to calculate and plot these functions on the positive real axis. We can re-express Eq. (79) as

$$J_{ij}(\omega) = \frac{1}{\pi}\int_0^{\infty} K_{aiaj}(s)\cos\omega s\, ds. \tag{83}$$

These functions can be evaluated explicitly using Eqs. (75), (76), and (78) to give

$$\begin{aligned} J_{11}(\omega) &= \frac{1}{\pi}\int_0^{\infty} K_{a_1a_1}(s)\cos\omega s\, ds \\ &= \frac{1.44261}{N_0\pi}\int_0^{\infty} e^{\lambda_f s}\ \cos\omega s\ ds \\ &\quad + \frac{0.22406}{N_0\pi}\int_0^{\infty} e^{\lambda_s s}\cos\omega s\, ds \\ &= \frac{1.44261}{N_0\pi}\frac{\lambda_f}{\lambda_f^2+\omega^2} + \frac{0.22406}{N_0\pi}\frac{\lambda_s}{\lambda_s^2+\omega^2}; \end{aligned} \tag{84}$$

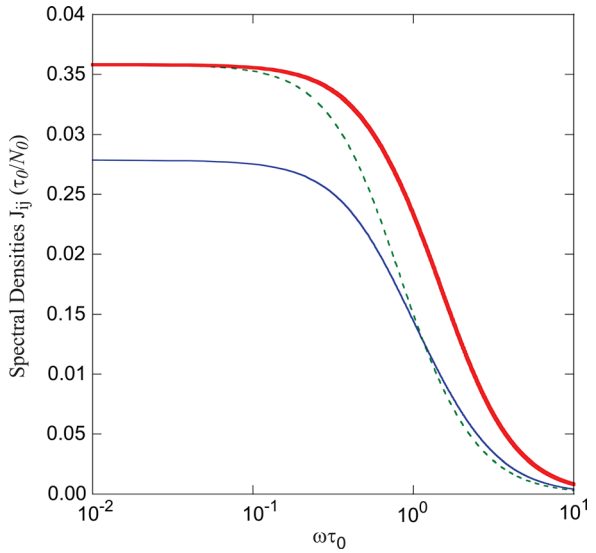

Fig. 10. Spectral density functions $J_{11}(\omega)$ (thick solid curve), $J_{12}(\omega) = J_{21}(\omega)$ (thin solid curve), and $J_{22}(\omega)$ (dashed curve). The spectral density scale is expressed in units of τ_0/N_0. The angular frequency scale is expressed in units of τ_0^{-1} with τ_0 given in Eq. (46).

$$J_{21}(\omega) = J_{12}(\omega) = \frac{1}{\pi}\int_0^\infty K_{a_1a_2}(s)\cos\omega s\, ds = \frac{0.58704}{N_0\pi}\frac{\lambda_f}{\lambda_f^2+\omega^2} + \frac{0.41296}{N_0\pi}\frac{\lambda_s}{\lambda_s^2+\omega^2}; \tag{85}$$

$$J_{22}(\omega) = \frac{1}{\pi}\int_0^\infty K_{a_2a_2}(s)\cos\omega s\, ds = \frac{0.23888}{N_0\pi}\frac{\lambda_f}{\lambda_f^2+\omega^2} + \frac{0.76112}{N_0\pi}\frac{\lambda_s}{\lambda_s^2+\omega^2}. \tag{86}$$

These functions are plotted in Fig. 10. We can interpret these functions as representing the amount of fluctuation, or noise, at a given frequency and within a narrow bandwidth. Though each of these functions has two cutoff frequencies, the frequencies are close enough together that a clear double-step shape to these curves is not observed. All of these functions fall off at high frequencies. We note that the noise in the energy variable a_1 goes out to larger frequencies than the noise in the particle number variable a_2. This is consistent with the energy transfer process being somewhat faster than the particle transfer.

The areas under these curves are related to the correlation functions by Eq. (80); setting $s = 0$ gives

$$\int_0^\infty J_{ij}(\omega)\, d\omega = \frac{1}{2}K_{a_ia_j}(0), \tag{87}$$

with values given by Eqs. (70)–(72).

Direct observation of these fluctuations in the readings from a standard pressure gauge on a typical-size vacuum chamber (say 50 l) near atmospheric pressure will likely be difficult. One might consider making the chambers as small as possible and conduct the experiments at lower pressures, i.e., make N_0 small.

XI. CONCLUSIONS

After briefly reviewing the nonequilibrium formalism for the Onsager symmetry relations and the linear equations for the approach to equilibrium, we have discussed in detail the kinematics of the effusion process. By linking the basic thermodynamics to the specific ideal gas kinetics, we explicitly verified the Onsager symmetry that we set out to test. This gives students of nonequilibrium thermodynamics a concrete example to supplement the general thermodynamic proofs available for the Onsager symmetry relations. Following this, we continued with example calculations for initial condition dynamics. These examples led to a frank assessment of the usefulness of Prigogine's stationary states. While the assessment is mostly negative, some insights are gained into how some systems with highly disparate timescales may benefit greatly from the stationary-state analysis. This discussion was followed by calculations for the correlation functions and noise spectral functions for this system. Example calculations of correlation functions and spectral densities for multi-variable systems are often left out of textbooks on this subject, so inclusion of these calculations is also beneficial for pedagogical reasons.

Also included was some brief discussions about how to experimentally test these results using standard vacuum technology. These calculations could be used to help understand and better design precision variable-leak valves used in many vacuum systems. It is hoped that the calculations discussed here will be beneficial to students of statistical mechanics and non-equilibrium thermodynamics. Additional exercises for students could be designed by using variables transformed away from the ones used here, such as can be found from diagonalizing the **G** matrix. Further example problems that verify the Onsager symmetry relations could be developed by looking into non-ideal gases and quantum gases (obeying either Fermi or Bose statistics) as well as looking into particle transfer processes other than effusion.

ACKNOWLEDGMENTS

The author thanks Cathy J. Meyer for her assistance in editing the manuscript.

[a]Electronic mail: steve.patitsas@uleth.ca; http://scholar.ulethbridge.ca/patitsas

[1]William Thomson, *Mathematical and Physical Papers*, Vol. 1 (Cambridge U.P., Cambridge, 1882), Article XLVIII.
[2]Hermann von Helmholtz, "Bericht über Versuche des Hrn. Dr. E. Root aus Boston, die Durchdringung des Platins mit elektrolytischen Gasen betreffend," Ann. Phys. Chem. **2**, 416–421 (1876).
[3]Lars Onsager, "Reciprocal relations in irreversible processes. I.," Phys. Rev. **37**, 405–426 (1931).
[4]Lars Onsager, "Reciprocal relations in irreversible processes. II.," Phys. Rev. **38**, 2265–2279 (1931).
[5]H. B. G. Casimir, "On Onsager's principle of microscopic reversibility," Rev. Mod. Phys. **17**, 343–350 (1945).
[6]S. R. de Groot, "Sur la thermodynamique de Quelques processus irreversibles I. Corps simples," J. Phys. Radium **8**, 188–191 (1947).
[7]H. B. Callen, "The application of Onsager's reciprocal relations to thermoelectric, thermomagnetic, and galvanomagnetic effects," Phys. Rev. **73**, 1349–1358 (1948).
[8]S. R. de Groot, "On the thermodynamics of the fountain phenomenon in liquid helium II and its inverse effect," Physica **13**(9), 555–557 (1947).
[9]Donald G. Miller, "Thermodynamics of irreversible processes—the experimental verification of the Onsager reciprocal relations," Chem. Rev. **60**, 15–37 (1960).
[10]S. R. de Groot, *Thermodynamics of Irreversible Processes* (North-Holland, Amsterdam, 1966), Chapter 3.
[11]I. Prigogine, *Introduction to Thermodynamics of Irreversible Processes* (Wiley, New York, 1967).

[12]E. T. Jaynes, "The minimum entropy production principle," Ann. Rev. Phys. Chem. **31**, 579–601 (1980).
[13]F. Reif, *Fundamentals of Statistical and Thermal Physics* (McGraw-Hill, New York, 1965), Chapter 15.
[14]L. D. Landau and E. M. Lifshitz, *Statistical Physics, Part 1* (Elsevier, New York, 1980).
[15]Neil W. Ashcroft and N. David Mermin, *Solid State Physics* (W. B. Saunders, Philadelphia, 1976), Chapter 13.
[16]Richard P. Wendt, "Simplified transport theory for electrolyte solutions," J. Chem Ed. **51**(10), 646–650 (1974).
[17]Daniel V. Schroeder, *An Introduction to Thermal Physics* (Addison-Wesley Longman, Don Mills, Ontario, 2000).
[18]William E. Boyce and Richard C. DiPrima, *Elementary Differential Equations*, 4th ed. (Wiley, Toronto, 1986).
[19]A. Roth, *Vacuum Technology*, 3rd ed. (North-Holland, New York, 1990).
[20]P. Maraghechi, S. A. Horn, and S. N. Patitsas, "Site selective atomic chlorine adsorption on the Si(111)7x7 surface," Surf. Sci. Lett. **601**, L1–L4 (2007).
[21]F. Reif and R. F. Knacke, *Solutions to Problems of "Fundamentals of Statistical and Thermal Physics"* (McGraw-Hill, New York, 1965).
[22]Mayo Martínez-Kahn and León Martínez-Castilla, "The fourth law of thermodynamics: The law of maximum entropy production (LMEP)," Ecol. Psychol. **22**(1), 69–87 (2010).

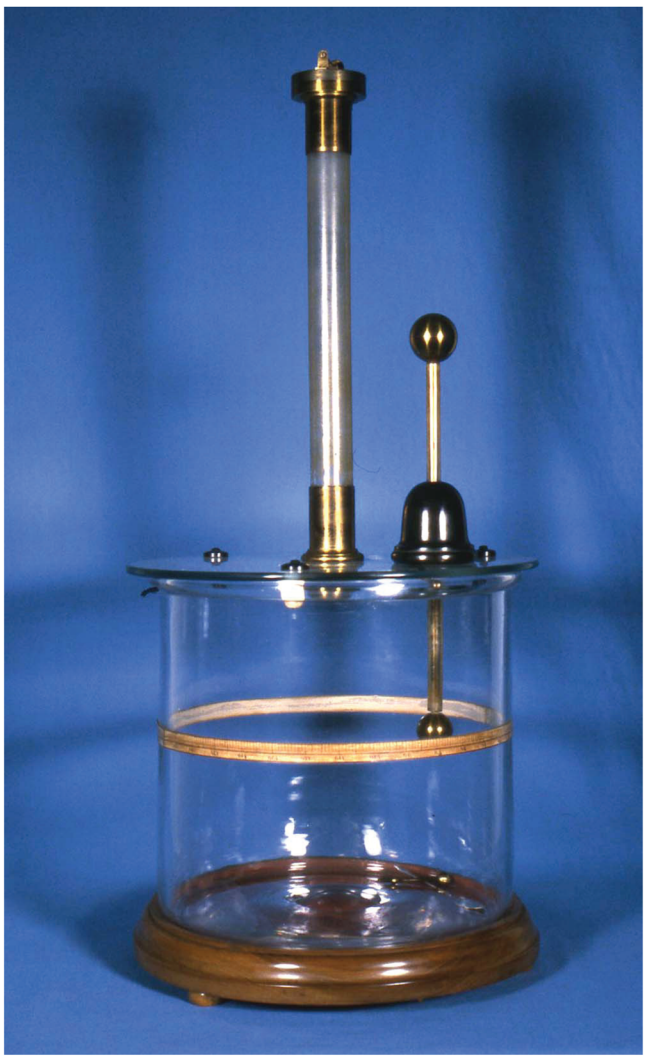

Coulomb Balance

The torsion balance has been used since the latter part of the 18th century to investigate the small electrostatic forces between two small charged bodies. Charles Coulomb (1736-1806) used the balance to make the first useful measurements leading to the formulation of the force law named after him. One charge is placed on the brass sphere on the bottom of the insulated rod inserted from the top of the apparatus, The other charge (of the same sign) is on a second small conducting sphere placed on the end of the counterbalanced crossbar, suspended by a torsion fiber. The use of the balance is easy in principle and difficult in actual practice, and one wonders how often the instruments were used by students. This example is in the collection of Yale University. (Notes and photograph by Thomas B. Greenslade, Jr., Kenyon College)